Modeling rammed earth wall using discrete element method

Bui, T.T. , Bui, Q.B. , Limam, A. and Morel, J. C.

Original citation & hyperlink:
Bui, T.T. , Bui, Q.B. , Limam, A. and Morel, J. C. (2015) Modeling rammed earth wall using discrete element method. Continuum Mechanics and Thermodynamics, volume 28 (1): 523-538
http://dx.doi.org/10.1007/s00161-015-0460-3

DOI 10.1007/s00161-015-0460-3
ISSN 0935-1175
ESSN 1432-0959

Publisher: Springer

The final publication is available at Springer via http://dx.doi.org/10.1007/s00161-015-0460-3 .

Modeling rammed earth wall using discrete element method

T.-T. Bui [1*], Q.-B. Bui [2], A. Limam [1*], J.-C. Morel [3]

[1] *Université de Lyon, INSA de Lyon, LGCIE, 69621 Villeurbanne Cedex, France.*

[2] *Université de Savoie, Polytech Annecy-Chambéry, LOCIE, CNRS, 73376 Le Bourget du Lac, France.*

[3] *Coventry University, Faculty of Engineering, Environment and Computing, School of Energy, Construction and Environment*

** Corresponding author:*

E-mail address: ali.limam@insa-lyon.fr

tan-trung.bui@insa-lyon.fr

ac0969@conventry.ac.uk

Abstract

Rammed earth is attracting renewed interest throughout the world thanks to its "green" characteristics in the context of sustainable development. Several research studies have thus recently been carried out to investigate this material. Some of them attempted to simulate the rammed earth's mechanical behavior by using analytical or numerical models. Most of these studies assumed that there was a perfect cohesion at the interface between earthen layers. This hypothesis proved to be acceptable for the case of vertical loading, but it could be questionable for horizontal loading. To address this problem, discrete element modeling seems to be relevant to simulate a rammed earth wall. To our knowledge, no research has been conducted thus far using discrete element modeling to study a rammed earth wall. This paper presents an assessment of the discrete element modeling's robustness for rammed earth walls. Firstly, a brief description of the discrete element modeling is presented. Then, thirteen parameters that were necessary for discrete element modeling were identified. The relevance of the model and the material parameters were assessed by comparing them with experimental results from the literature. The results showed that, in the case of vertical loading, interfaces did not have an important effect. In the case of diagonal loading, model with interfaces produced better results. Interface's characteristics can vary from 85% to 100% of the corresponding earthen layer's characteristics.

Keywords: rammed earth, discrete element method, interface characteristics

1 Introduction

Rammed earth (RE) materials are ideally composed of sandy-clayey gravels which are compacted inside a temporary formwork to manufacture walls. Clay acts as the binder between the grains and a mixture of silt, sand, and gravel up to a few centimeters in diameter. Material that has been prepared for optimum moisture content, i.e., to provide the highest

dry density for the energy used, is then compacted (Bui *et al.* 2009 [4]). The RE wall is composed of several layers of earth which are rammed manually or pneumatically in a timber or metal formwork. After compaction, the thickness of each layer is typically 8–10 cm. The procedure is repeated until completion of the wall. A detailed presentation of RE construction can be found in Walker *et al.* (2005) [31].

RE is now the focus of scientific research for two main reasons. Firstly, in the context of sustainable building, the interest in earth as a building material is largely derived from its low embodied energy, both for unstabilized (Morel *et al.* 2001 [23]) and stabilized RE (Reddy and Kumar 2010 [25]), and also because the material has a good natural moisture-buffering capacity for indoor environments (Allinson and Hall 2010 [1]). Secondly, the heritage of RE buildings in Europe and the world is still important (Fodde 2009 [17], Bui *et al.* 2009 [3]). Maintaining this heritage requires scientific knowledge to assess appropriate renovations.

Several investigations have recently been conducted to study the mechanical characteristics of RE by using analytical methods ([4], [5], [6], [11], [12], [13], [21]) or by employing a numerical model ([9], [18]). These studies assumed that the cohesion at the interface between earthen layers was perfect. This hypothesis proved to be acceptable for the case of vertical loading [7], but it could be questionable for horizontal loading. To address this problem, discrete element modeling (DEM) seemed to be a relevant means of simulating a RE wall. To our knowledge, no study has used DEM to study RE walls. Therefore, this paper presents an assessment of the DEM's robustness in the case of RE walls. Firstly, a brief description of the DEM is presented. Then, parameters necessary for the DEM are determined. The relevance of the model is assessed by comparing the findings with experimental results from the literature. The results showed that, in the case of vertical loading, interfaces did not have an important effect. In the case of diagonal loading, model with interfaces produced better results. Interface's characteristics can vary from 85% to 100% of the corresponding earthen layer's characteristics. Thus, in practice, model without interfaces can also be used, because results are sufficiently precise and can be calculated faster.

2 Discrete element method

An explicit DEM based on finite difference principles originated in the early 1970s as the result of landmark work on the progressive movements of rock masses as 2D rigid block assemblages (Cundall, 1971 [15], [16]). This technique was then extended to the modeling of masonry structures ([8], [10], [24]; [29]) and concrete structures [28]. To our knowledge, however, no research has thus far used DEM to study RE walls.

The 3DEC (3-Dimensional Distinct Element Codes [19]) was used in this study. The RE wall was modeled as an assemblage of discrete blocks (earthen layers), and the interfaces between earthen layers were modeled by introducing an interface law. The behavior of these elements will be described in the following sections.

2.1 Constitutive behavior of earthen layers (blocks)

Earthen layers were assumed to be homogeneous, isotropic and were modeled by blocks which were further divided into a finite number of internal elements for stress, strain, and displacement calculations. The failure envelope used in this study was the Mohr-Coulomb criterion with a tension cut-off. This model existed in the discrete element code; its relevance was checked in the case of masonry walls [20].

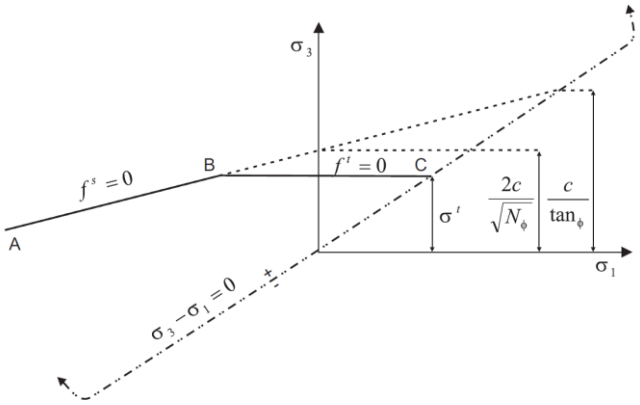

Figure 1: Mohr-Coulomb failure criterion used (Itasca 2011 [19])

The Mohr-Coulomb criterion is expressed in terms of the principal stresses σ_1, σ_2, and σ_3, which constitute the three components of the generalized stress vector for this model (n = 3), whereby the three principal stresses are: $\sigma_1 \leq \sigma_2 \leq \sigma_3$. Components of the corresponding generalized strain vector are the principal strains ε_1, ε_2, ε_3. This criterion can be represented in the plane (σ_1, σ_3), as illustrated in Figure 1 (compressive stresses are negative). The failure envelope f(σ_1, σ_3) = 0 is defined from point A to B by the Mohr-Coulomb shear failure criterion $f^s = 0$ with $f^s = \sigma_1 - \sigma_3 N_\varphi + 2c\sqrt{N_\varphi}$; and from B to C by a tensile failure criterion of the form $f^t = 0$ with $f^t = \sigma_3 - \sigma_t$; where φ is the friction angle, c is the cohesion, σ_t is the tensile strength, and $N_\varphi = \frac{1+\sin\varphi}{1-\sin\varphi}$.

Note that the tensile strength of the material cannot exceed the value of σ_3 corresponding to the intersection point of the straight lines $f^s = 0$ and $\sigma_1 = \sigma_3$ in the (σ_1, σ_3) plane. This maximum value is given by $\sigma^t_{max} = \frac{c}{\tan\varphi}$. The potential function, g^s, used to define shear plastic flow, corresponds to a non-associated law according to the equation $g^s = \sigma_1 - \sigma_3 N_\psi$, where ψ is the dilation angle and $N_\psi = \frac{1+\sin\psi}{1-\sin\psi}$.

If shear failure takes place, the stress point is placed on the curve $f^s = 0$ using a flow law which is derived by using the potential function g^s. If tensile failure is declared, the new stress point is simply reset to conform to $f^t = 0$ (Figure 1); no flow rule is used in this case.

2.2 Constitutive behavior of interfaces

The interfaces between earthen layers were modeled by an interface law between the blocks following the Mohr-Coulomb interface model with a tension cut-off. This interface constitutive model considers both shear and tensile failure, and interface dilation is included. In the elastic range, the behavior is governed by normal and shear stiffness of the interface, k_n and k_s :

$$\{\sigma\} = [K]\{u\} \quad \text{or} \quad \begin{Bmatrix} \tau_s \\ \sigma_n \end{Bmatrix} = \begin{bmatrix} k_s & 0 \\ 0 & k_n \end{bmatrix} \begin{bmatrix} u_s \\ u_n \end{bmatrix} \quad (1)$$

where: σ_n : normal loading; u_n : normal displacement

τ_s : shear stress; u_s :shear displacement.

The maximum shear force allowed is given by: $\tau_{max} = c + \sigma_{n(max)} . \tan \varphi$ (2)

where c and φ are the interface cohesion and friction angle. After this peak, shear strength drops until a residual strength τ_{res} (Figure 2a), with: $\tau_{res} = \sigma_{n(max)} \tan \varphi$ (3)

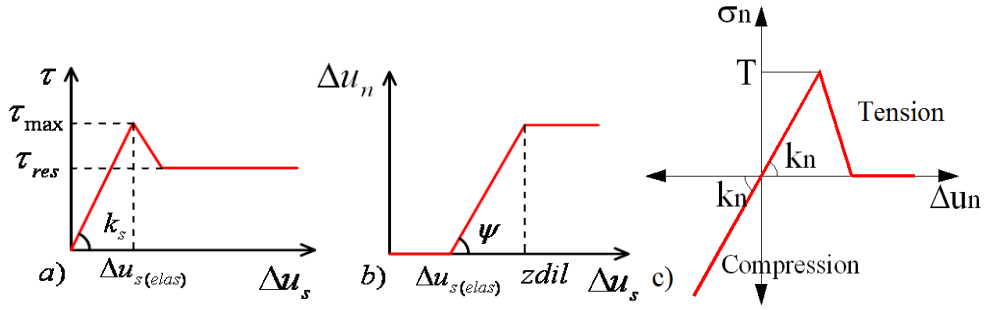

Figure 2: Interface behavior: a) Mohr-Coulomb slip model; b) Bilinear dilatant model; c) Behavior under uniaxial loading.

As indicated in Figure 2b, the interfaces begin to dilate when the interface fails in shear, at $\Delta u_{s(elas)}$ shear displacement. This displacement leads to a dilatation of:

$$\Delta u_{n,dilatation} = \Delta u_s tan\psi \quad (4)$$

where ψ is the dilatancy angle.

The normal stress must be corrected to take the effect of dilatation into account:

$$\sigma_{n,total} = \sigma_{n,elastic} + \sigma_{n,dilatation} = k_n.\Delta u_n + k_n.\Delta u_{n,dilatation} = k_n.\Delta u_n + k_n.\Delta u_s tan\psi \quad (5)$$

When a dilatation is presented, the shear displacement is in the plastic phase ($\Delta u_s > \Delta u_{s(elas)}$, Figure 2a). The normal displacement is assumed linear until z_{dil} (Figure 2b). Dilatation increases if the shear displacement increment runs in the same direction as the total shear displacement and decreases if the shear increment runs in the opposite direction.

The extension occurs until the limiting shear displacement (z_{dil}) is reached. The interface behavior under uniaxial loads is plotted in Figure 2c, where T is the interface tensile strength. Before the tensile failure ($\sigma_n < T$), an elastic behaviour is assumed.

3 Identification of Mohr-Coulomb's parameters used in the DEM

Thirteen parameters need to be identified for the model:

- For the earthen layer (7 parameters): density D, Young modulus E_{layer}, Poisson's ratio ν, tensile strength $f_{t,layer}$, cohesion c_{layer}, friction angle φ_{layer}, and dilatancy angle Ψ_{layer} ;
- For the interface (6 parameters): normal stiffness k_n, tangent stiffness k_s, tensile strength $f_{t,interface}$, cohesion $c_{interface}$, friction angle $\varphi_{interface}$, and dilatancy angle $\Psi_{interface}$

Among the aforementioned parameters, several characteristics of the earthen layer can be directly or indirectly found in the literature (density: Bui et al. 2009 [4]; Young's modulus: Bui et al. [4], [7]; Poisson's ratio: Bui et al. 2014 [7]; tensile strength and cohesion: Bui et al. 2014 [9]; friction angle: Cheah et al. 2012 [11], Bui et al. 2014 [9]; and dilatancy angle: Vermeer et al. 1984 [30]), which will be detailed in the next sections. However, parameters concerning the interface have not been reported previously. This study has identified these 13 parameters. The first step was to determine the interface's elastic stiffness (normal stiffness and tangent stiffness) by using the results of in situ nondestructive measurements. The next step was to identify the other parameters using the results of laboratory destructive tests.

3.1 Identification of the interface's elastic stiffness

First, during the manufacture processing, earth is at a "wet" state which corresponds to the optimum water content, so cohesion between the earthen layers is developed. Then, in normal conditions, RE wall principally works in compression due to its own weight and the vertical loads. These are the reasons why the theory of elasticity can be assumed for an interface element in the case of small loading (Lourenço *et al.*, 2005 [20]).

Theoretically, by applying a classical homogenization method (see Bui et al. 2009 [4] or Lourenço et al. 2005 [20]), the interface's elastic stiffness could be determined from the Young modulus and shear modulus of the wall and the earthen layer (block):

$$k_n = \frac{E_w \cdot E_{layer}}{(E_{layer} - E_w) \cdot h_{layer}} \quad (6)$$

$$k_s = \frac{G_w \cdot G_{layer}}{(G_{layer} - G_w) \cdot h_{layer}} \quad (7)$$

where E_w , G_w are the Young and shear modulus of RE wall

E_{layer} , G_{layer} are the Young and shear modulus of an earthen layer (block), and

h_{layer} is the thickness of an earthen layer

Following the theory of elasticity (Lourenço et al. 2005 [20]): $G = E / [2(1+\nu)]$ (8)

Therefore: $k_n = 2(1+\nu)k_s$ (9)

The Young and shear modulus of a RE wall can be determined experimentally (e.g., see Bui et al. [4], [7], Silva et al. [26]). However, determining the characteristics of an earthen layer is a very delicate operation because it is difficult to manufacture and test a sample which represents only an earthen layer of RE. Bui et al. (2009) discussed this in their study [4].

For this reason, another method was used to determine the interface's stiffness. In fact, normal and tangent stiffness of interfaces represent elastic characteristics so that they can be identified in an elastic domain. Therefore, the results from *in-situ* non-destructive tests can be used to identify these parameters. Wall no. 1 in Bui et al. (2009) [4] was chosen to be modeled, which was a RE wall 2.3 m in height built on a concrete base of 0.3 m (Figure 3).

In that study, accelerometers were placed on the top and at the base of the wall, which made it possible to measure both the accelerations in two horizontal axes and the torsional movement of the wall. After data processing based on the theory of structural dynamics, the wall's natural frequencies were identified. From these natural frequencies, the wall's Young modulus could be determined following the relationship (Clough and Penzien [14]):

$$frequency = function(dimensions, Poisson's\ ratio)\sqrt{\frac{Young's\ modulus}{density}} \qquad (10)$$

More details can be found in Bui et al. [4].

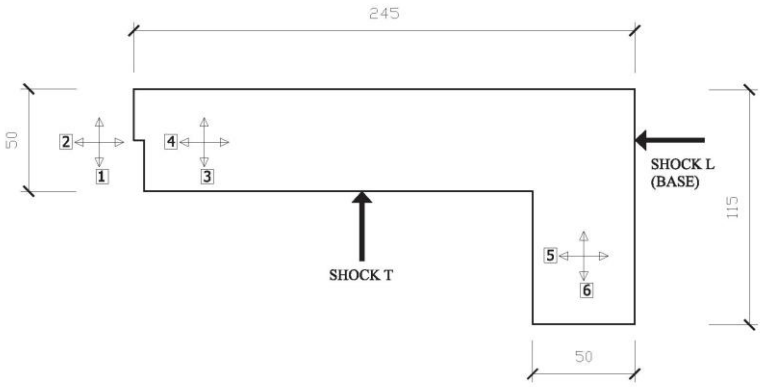

Figure 3: Sensor layout on wall No. 1 and shock directions (dimensions in centimeters)

That study (Bui et al. 2009 [4]) showed that, with respect to the wall's moisture content, density varied from 19.5 to 20.3 kN/m^3 and the Young modulus varied from 440 to 470 MPa,. In the present study, the wall was modeled at quasi-dry state, which corresponded to a density and Young modulus of 19.5 kN/m^3 and 470 MPa, respectively (Figure 4). The compressive strength was determined by compression tests in the laboratory, which gave f_c = 1.0 MPa. The Poisson ratio ν reported by Bui et al. 2014 [7] for the case of quasi-dry specimens was equal to 0.22.

The other parameters are less important in this case because the strains were small during dynamic measurement. The identification of those parameters will be presented in detail in the following section of this paper. The following values were used: cohesion and tensile strength of the earthen layer: $f_{t,layer} = c_{layer} = 0.1\ f_c$ (Bui et al. 2014 [9]); friction angle of the earthen layer φ_{layer}=45° (Cheah et al. 2012 [11]); and dilatancy angle Ψ_{layer}=12° (Vermeer et al. 1984 [30]). For the cohesion, tensile strength, and friction angle of the interface, a parametric study has been firstly performed and then they were taken at 85% of the respective values of earthen layer; this ratio will be justified in the next sections; dilatancy angle of interface =12°.

(a)  (b) 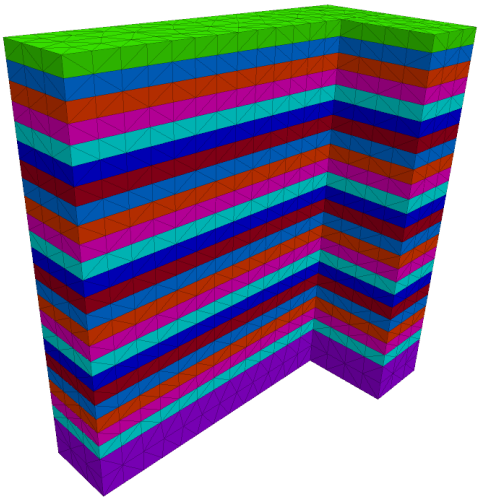

Figure 4: Wall No. 1 (a) and its mesh in DEM (b)

A technique by which the interface stiffness can be determined from measured frequencies was developed and presented by Bui *et al.* (2014) [10]. The principle of this technique was that, in the DEM model, the wall was excited by a weak shock. The dynamic response at a top point of the wall was recorded and analyzed (Figure 5). The natural frequencies were identified by transforming data from the time domain (Figure 5) to the frequency domain using the FFT (Fast Fourier Transform). The peaks in the frequency domain correspond to the natural frequencies of the structure. Each natural frequency corresponds to a vibrational mode.

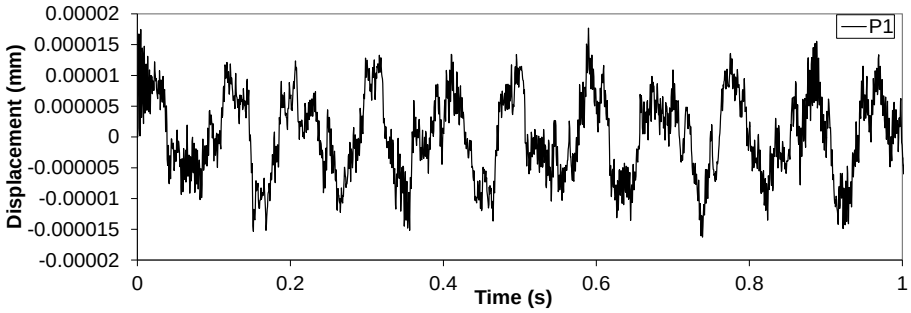

Figure 5. Recorded vibration of the top point P1 in a horizontal direction after impact.

Table 1: Comparison of frequencies obtained by DEM and by measurement

Modes	**f_{model} (Hz)**	**$f_{measured}$ (Hz)**	**f_{model} / $f_{measured}$**
1	10.8	10.8	1.00
2	17.3	18.2	0.95
3	23.1	24.0	0.96
4	36.8	36.5	1.01

A parametric study was performed to study the variation in the model frequencies as a function of the interface stiffness (k_n and k_s). The value of k_n (so k_s), which reproduced the first measured frequency (the most important frequency), was selected; the correlation of other frequencies was also checked (for more information, see Bui *et al.* (2014) [10]). A stiffness of k_n = 60GPa/m (so k_s=24.6GPa/m) was selected and the corresponding frequencies are presented in the Table 1.

3.2 Identification of the earthen layer's parameters

Following previous studies (Bui et al. [4], [5], [9]), the presence of an interface did not have an important influence on the behavior of walls under vertical load. Therefore, the aim of this section of the present study is firstly to confirm this point; and then, when the influence of interface parameters is showed negligible under vertical load, the parameters of the earthen layer will be identified.

Two walls tested in the previous study (Bui et al. 2014 [9]) were used to identify the parameters in compression. These walls measuring (100 × 100 × 30) cm^3 were subjected to concentrated loads on a (30×30) cm^2 surface at the middle of the wall parameters (Figure 6).

In that study, the walls were modeled by using the finite element method (FEM), which assumed that the link between earthen layers was perfect (homogeneous material). That model could reproduce the maximum experimental load and the failure mode of the first cracks but it could not reproduce the failure displacement (corresponding to the maximum load) and the last cracks (failure).

By using DEM, the robustness of DEM and FEM can be compared in the present study. In order to assess the influence of interfaces, two DEM models were studied:

- Model without interface (homogeneous material) (Figure 6b)
- Model with interface (Figure 6c)

The contact between the RE wall and the concrete base was modeled by a contact which follows the Mohr-Coulomb law and had a friction angle of 15° (usual value for concrete surface).

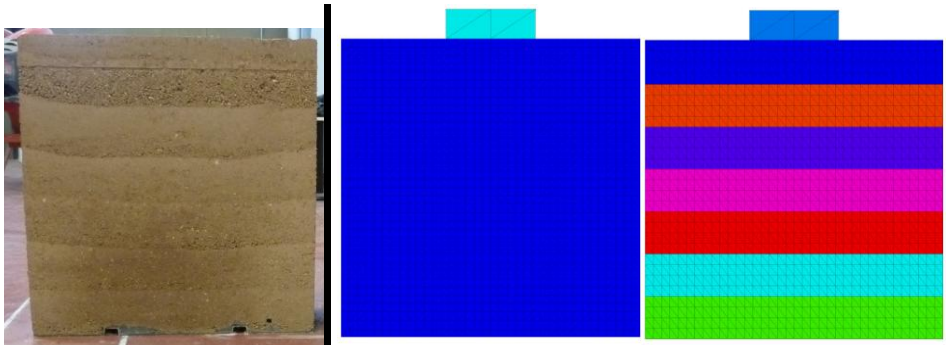

(a) (b) (c)

Figure 6: a) Wall studied; b) c) Model without and with interfaces.

3.2.1. Influence of interfaces in compression test

Following the previous study, the experimental compressive and tensile strengths of earthen layers were f_c=1.3MPa and $f_{t,layer}$ = 0.13MPa, respectively. For the other parameters, the following experimental values were found in the literature:

- A cohesion of the earthen layer that equals 7-10% of the compressive strength of the earthen layer: c_{layer} = 0.07-0.1 f_c (7% following New Zealand Standard (design value) [27] and 10% following Bui et al. 2014 [9]) can be taken; friction angle of earthen layer can vary from 45 to 56° : φ=45-56° (45-56° following Cheah et al. 2012 [11]; 51° following Bui et al. 2014 [9]); dilatancy angle of earthen layer Ψ_{layer}=12° (following Vermeer et al. 1984 [29]: dilatancy angle of clay 0°; concrete 12°; granulated and intact marble 12°-20°; dense sand 15°; loose sand < 10°; thus in the case of RE, a dilatancy angle of 12° can be taken). According to a preliminary study, the dilatancy angle did not play an important role in RE walls.
- cohesion, tensile strength, and friction angle of interfaces could be estimated at about 85% of the respective values of the earthen layer. Indeed, in the study of Ciancio and Augarde (2013) [13], the tensile strength of the interface was about 85% of that of the earthen layer. The dilatancy angle of 12° of the interface could be taken because it did not play an important role here.

Nevertheless, in order to assess the influence of the interface in this case, low values of cohesion, tensile strength, and friction angle of interfaces were chosen for the model, which were 25% of the respective values of earthen layers. The cohesion and friction angle of earthen layers of c_{layer}=10%f_c and φ_{layer}=45°, respectively, were chosen. The sensitivity of these parameters will be discussed in the next section. The synthesis of the parameters used is presented in Table 2. A comparison of the results is illustrated in Figure 7, Figure 8, and Figure 9. These results show that even with very low interface parameters, the results obtained by models with or without interfaces were similar. That confirms that interfaces do not significantly affect vertical loading.

Table 2: Parameters of earthen layer and interface used to study the influence of interface in the case of vertical loading

Earthen layer						
Density	Young Modulus	Poisson ratio	Tensile strength	Cohesion	Friction angle	Dilatancy angle
d (kg/m^3)	E (MPa)	ν	f_t =10%fc (kPa)	C=f_t = 10%f_c (kPa)	φ (°)	ψ (°)
1950	500	0.22	130	130	45	12

Interface					
Normal stiffness	Tangent stiffness	Tensile strength	Cohesion	Friction angle	Dilatancy angle
k_n (GPa/m)	k_s (GPa/m)	$f_{t,\,inter}$ = 25% $f_{t\,,\,layer}$ (kPa)	C_{inter} = 25% C_{layer} (kPa)	φ (°)	ψ (°)
60	24.59	32.5	32.5	25	12

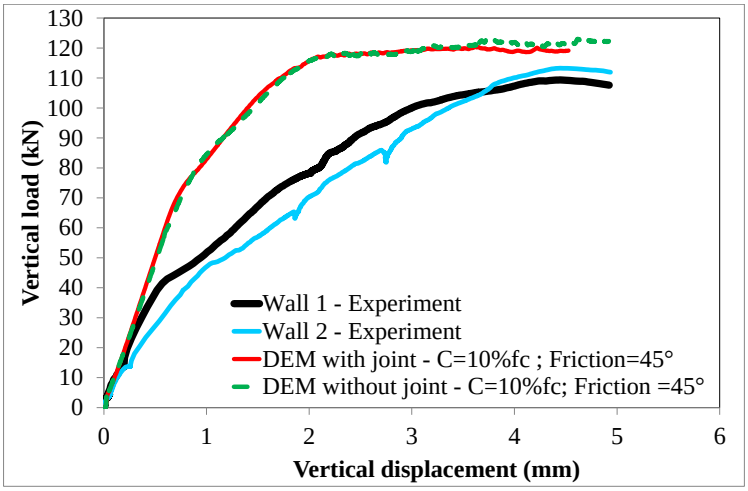

Figure 7: Comparison of the numerical and experimental results

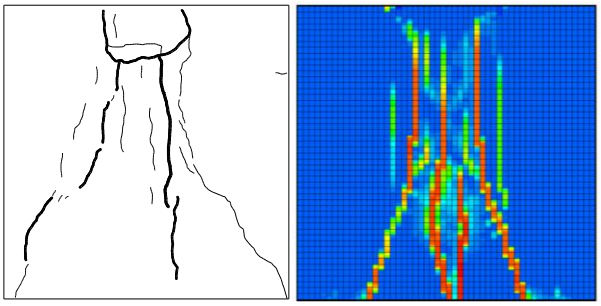

a) b)

Figure 8: Failure modes of the wall: a) experimental result; b) FEM with Mazars' damage model (Bui et al 2014a [9])

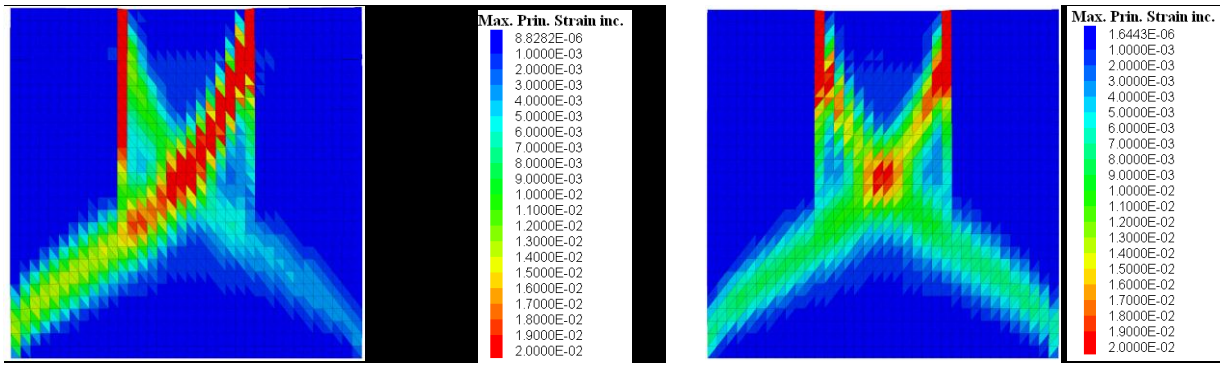

(a) (b)

Figure 9: Max principal strain in the numerical model (at 5mm vertical displacement): a) with interface = 25% layer; b) without interface.

Figure 9 shows that the DEM (with Mohr-Coulomb model) reproduces the failure mode better than the FEM (with Mazars' damage model, Figure 8b).

3.2.2. Assessing the cohesion and friction angle of earthen layers

Figure 7 shows that, with the chosen parameters, the maximal load for the numerical model was greater than that for the experimental model (about 10%). This difference may be due to the used parameters which were not yet optimized. As the interface could be neglected in this case, only the influence of the cohesion and friction angle of earthen layers was studied. Two cases were considered to optimize the numerical model:

- Friction angle was fixed at 45°; cohesion varied from 7% to 10% of the compressive strength: c_{layer} =(7% ;8% ;9% ;10%)f_c. The results are presented in Figures 10 and 11.
- Cohesion was fixed at 7% and 9% of the compressive strength, respectively; friction angle varied from 45° to 56°. The results are presented in Figures 12 and 13.

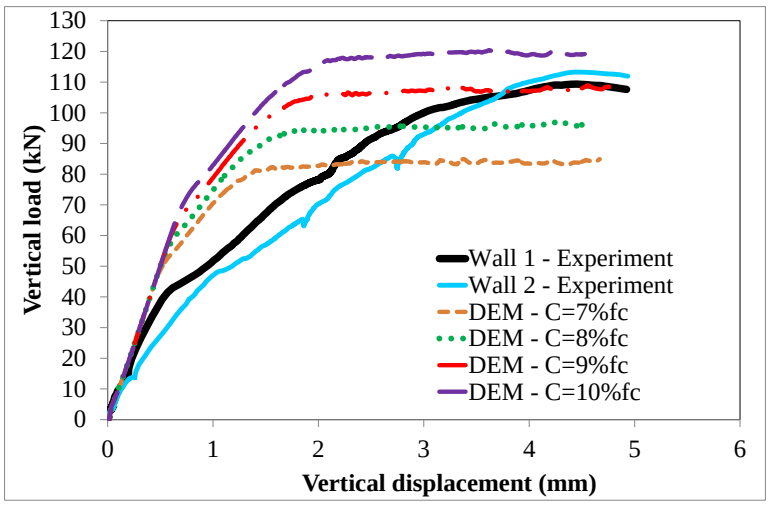

Figure 10: Comparison of the numerical and experimental results (φ_{layer}=45°)

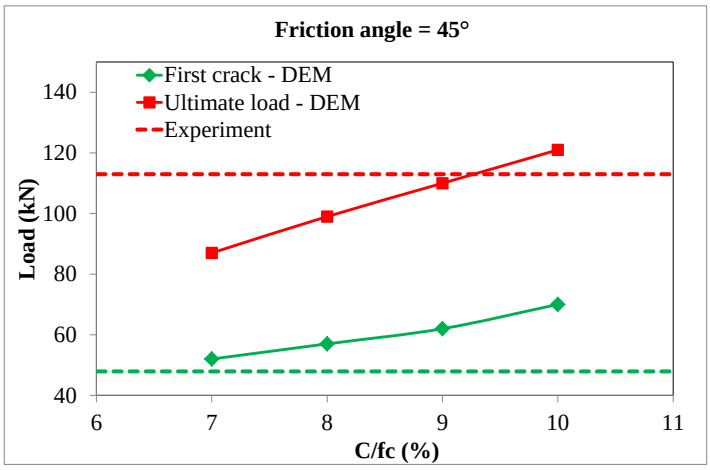

Figure 11: Influence of cohesion c_{layer} on the first crack load and ultimate load (φ=45°)

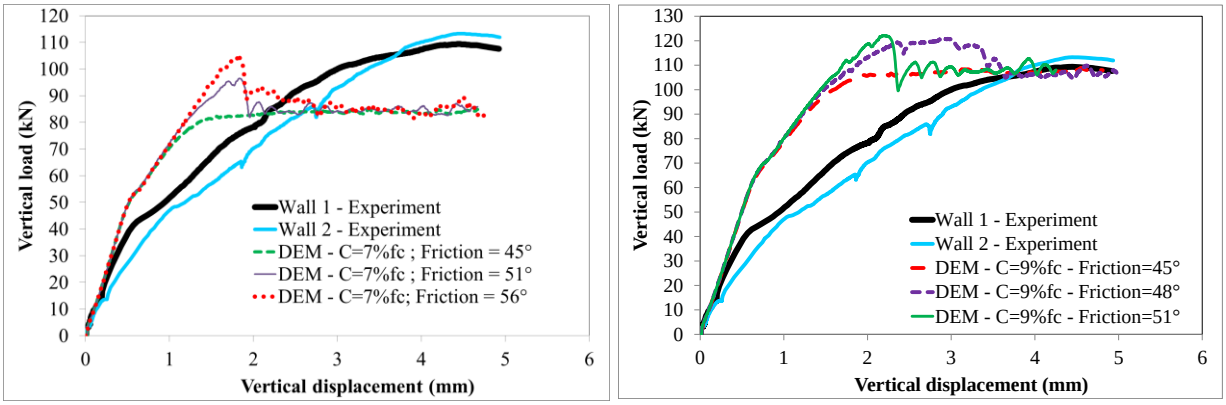

(a) **(b)**

Figure 12: Influence of the friction angle on the vertical load a) c_{layer}=7%f_c ; b) c_{layer}=9%f_c .

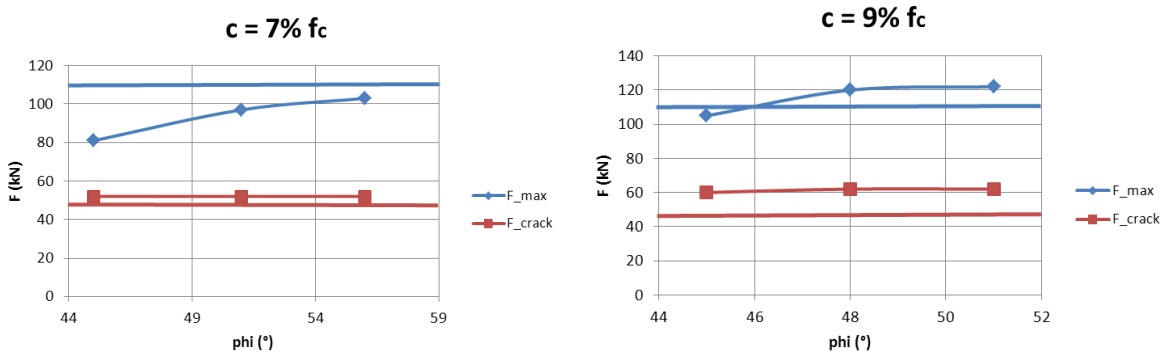

(a) (b)

Figure 13: Variation of first crack load and ultimate load in function of friction angle, a) c_{layer}=7%fc; b) c_{layer}=9%fc

From Figures 11 and 12, the best cohesion value for the layers is in the range 7 to 9%. Figure 13 shows that the friction angle does not play a significant role for the first crack load (which corresponds to the slope's change in Figures 10 and 12). However, it does affect the ultimate load. Figure 11 shows that the tensile strength has an effect on the first crack load and the ultimate load. When this parameter increases, the first crack and ultimate loads increase; the more important effect on the ultimate load can be observed.

From these results, the best pair of layer characteristics was c_{layer}=9% and φ_{layer}=48°, which gave the results closest to the experimental results: first crack load, ultimate load, and the post-peak mode. It is interesting to note that the used model can reproduce three phases of the walls' behavior: elastic, post-elastic and post-peak phases. However, there were still some differences in the experimental results, which may come from the limit of the models used for DEM (Mohr-Coulomb for earthen layers, tension cut-off for interfaces). However, the study could confirm the results presented in previous studies in which the layer's cohesion was about 7-10% of compressive strength and the layer's friction angle was about 50° (Bui et al. 2014 [9], Cheah et al. 2012 [11]).

3.3 Identification of cohesion and tensile strength of the interface

The results of diagonal compression tests presented in Silva et al. (2013) [26] were used to identify the cohesion and tensile strength of the interfaces. In that study, walls of 550x550x220mm^3 compacted in 9 layers were tested (schema in Figure 14). The testing procedure was similar to that of ASTM E519 [2], which consisted in applying a monotonic displacement of 4 µm/s and using supports of 100 mm in length. With a diagonal compression, the interface shear behavior was solicited more than for vertical loading, which made it possible to determine the characteristics.

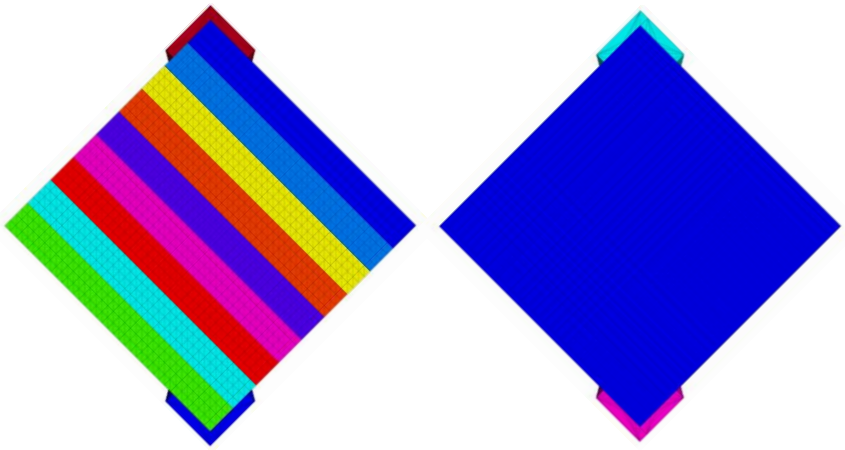

Figure 14: Model with and without interfaces.

The wall GSRE_7.5 was selected to be studied, i.e., granitic stabilized rammed earth with 7.5% of ash (by weight). This stabilization technique consisted in the alkaline activation of fly ash (stabilization by addition of a geopolymeric binder). The experimental results obtained in that study were: compressive strength f_c=1.09MPa; Young modulus E=2858MPa; shear strength τ=0.18MPa, and shear modulus G= 620MPa.

This wall was chosen, firstly, because its compressive and shear strengths were similar to that of currently unstablized RE. However, its elastic and shear modulus were greater than that of currently unstabilized RE (see Bui et al. 2014 [7], for example). This could be due to the effect of the stablization. Secondly, the failure mode of this wall was more complex than for other walls (GSRE_2.5 and GSRE_5). Further details about failure modes will be discussed later in this paper.

In order to assess the influence of interfaces, several cases were studied:

- Cohesion, tensile strength, and friction angle of interfaces were the same as earthen layers. This is equivalent to the case without interface.
- Cohesion, tensile strength, and friction angle of interfaces of 85% and 90% of the earthen layers, respectively, were taken. It is important to note that a preliminary study showed that lower values for interface parameters could not reproduce the experimental results in this case.

3.3.1. Model without interfaces

By taking the above results into account, in this case, the layer cohesion was 7% and 10% of the compressive strength (c_{layer}/f_c=7% and 10%), respectively; the friction angle varied from 45° to 56°. The results are presented in Figure 15, in which:

- Shear stress of the specimens was calculated: $\tau=\frac{0.707\times P}{A_n}$ (10)

  where P is applied load and An is the net area of the specimen.

- Shear distortion γ was obtained by: $\gamma = \frac{\Delta v}{g_v} + \frac{\Delta h}{g_h}$ (11)

  where Δv and Δh were vertical shortening and horizontal extension of the panel, respectively; g_v and g_h were vertical and horizontal gage lengths. In the DEM model, Δv and Δh were measured on two diagonal lines of the specimen .

From Figure 15, all models could reproduce the shear modulus of the wall, which was the slope of the first part of the test (until 20% of the ultimate shear stress). However, these models could not reproduce the slope's change after the first part of the test. Among these results, cohesion $c_{layer}=10\%f_c$ and friction angle $\varphi_{layer}=50°$ for the pair of layers gave the most adapted result for the ultimate shear strength. Therefore, these values were chosen for the model with interfaces to check whether this model could better reproduce the behavior of the wall after the first part of the test. This model could reproduce the diagonal crack of the experiment (Figure 16) but it could not yet reproduce the horizontal crack at the interface between the third and fourth layers (from the top).

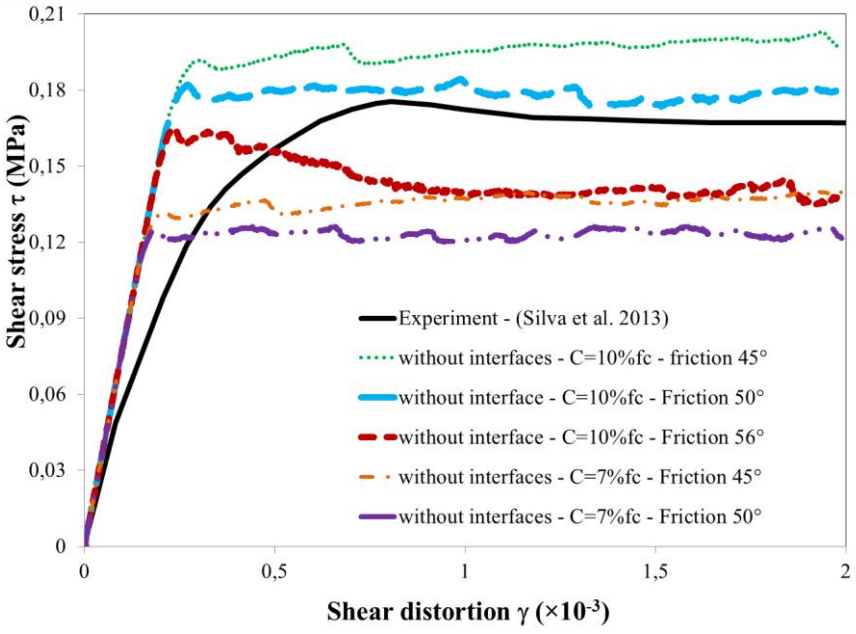

Figure 15: Comparison of the results of models without interfaces and those of the experiment.

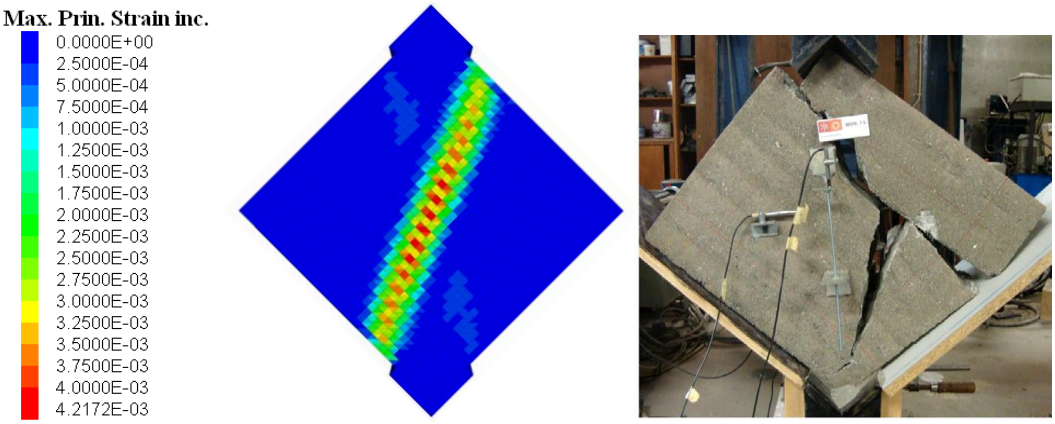

(a) (b)

Figure 16: a) Max principal strain in the model without interface; b) experimental failure [26]

3.3.2. Model with interfaces

As no study in the literature previously investigated the cohesion and the friction angle of the interface, a parametric study with several values was performed for the model with interfaces: interface cohesion $c_{interface}$ and friction angles $\varphi_{interface}$, respectively, of 70% ; 80% ; 85% , and 90% of the corresponding parameters of the earthen layer were taken.

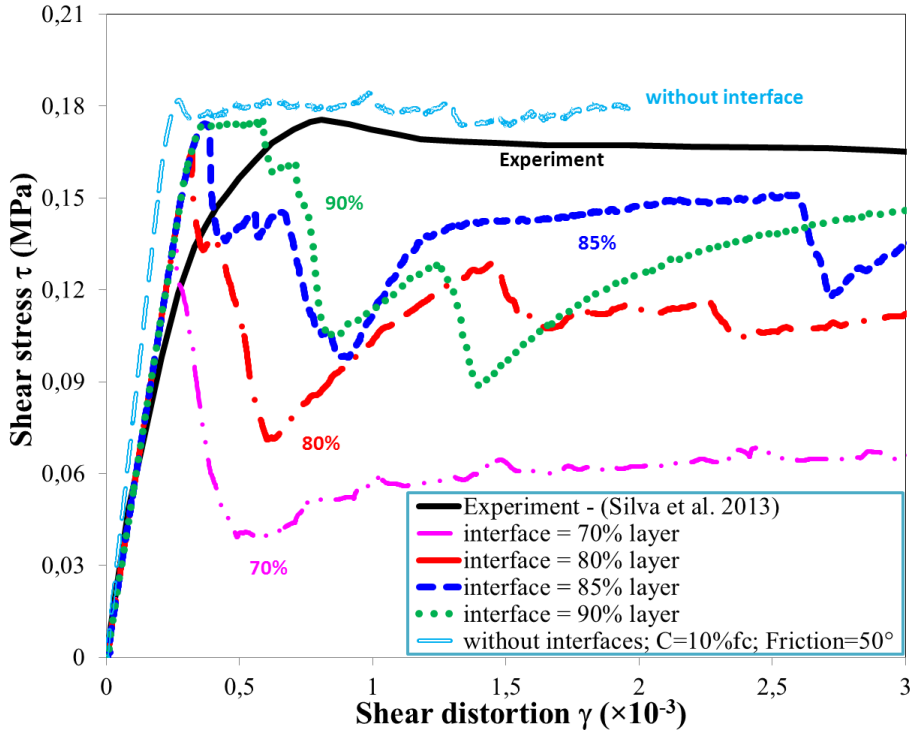

Figure 17: Comparison of the numerical and experimental results

The interface's elastic stiffness, k_n and k_s, which was determined in a previous part of the study by in situ dynamic testing (k_n=60GPa/m ; k_s=24.6GPa/m), was used. The validity of these values will be checked for this case.

The results are presented in Figure 17. It is observed that the models with interfaces could reproduce the first part of the experimental result up to 50% of the ultimate shear stress, which was better than the model without an interface (up to 20% of the ultimate shear stress). Among the models with interfaces, the model in which the interface's characteristics constituted 90% of the layers gave results closest to those of the experimental model. Indeed, the peak curve for this model was closest to the peak of the experimental curve, both for shear stress and shear distortion. However, none of the studied models could reproduce the nonlinear behavior of the experiment before the peak. This may be explained by the behavior law used for the interfaces (Figure 2), which is linear before the failure.

Nevertheless, when the failure modes were observed (Figures 18 and 19) the model with interfaces at 85% of the layer's characteristics was the one that could reproduce the failure at the interface of the third layer. The model with interfaces having 90% of the layer's characteristics could only reproduce the diagonal crack. For the model with interfaces having 70% of the layer's characteristics, the failure was a local failure of the interface that was not representative of the experiment.

These results show that a discrete model with interfaces having 85-90% of the layer's characteristics is the most relevant. This result is similar to that presented in the paper of Ciancio and Augarde (2013) [13], where the tensile strength at the interfaces was 85-90% of the tensile strength in earthen layers.

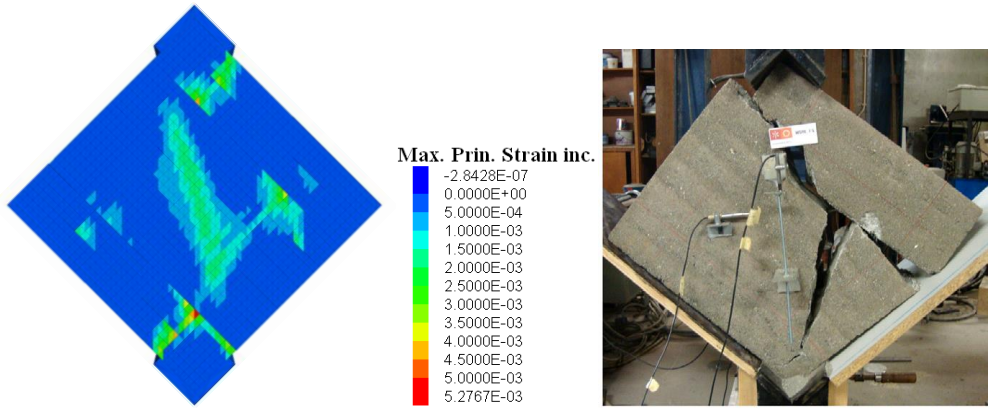

(a) (b)

Figure 18: a) model with interfaces, $c_{interface}$=85%c_{layer}; b) experimental failure [26]

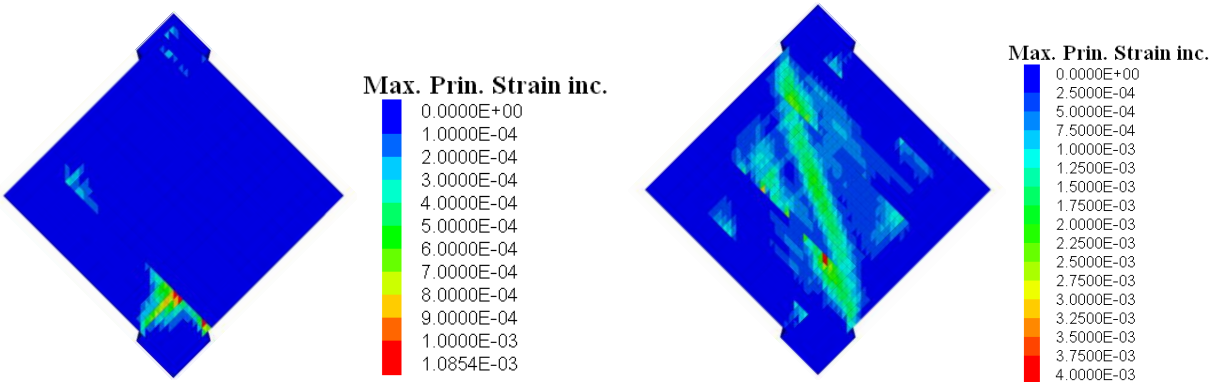

(a) (b)

Figure 19: Models with interfaces: a) $c_{interface}$=70%c_{layer} ; b) $c_{interface}$=90%c_{layer}

3.4 Discussion of the interface characteristics

The results of the models in which the interface's characteristics represented 90-100% of the layer's characteristics could reproduce the slope of the elastic part, the ultimate shear stress, and the diagonal crack of the experiment. This failure mode was observed on other walls in the study of Silva et al. (2013) [26],

Figure **20**. This means that the interface's characteristics can vary from 85% to 100% and still give satisfactory results. Hence, for an accurate result, the model with the interface is better but, in practice, the model without the interface can also give a sufficiently precise result and be calculated faster. The results of our study confirm the suprising result presented in Bui et al. 2014 [9], where the tensile strengths in earthen layers and at interfaces were similar.

(a) (b)

Figure 20: Failure mode of the wallets: (a) GSRE_2.5; (b) GSRE_5.0 (Rui et al. 2013)

4 Conclusions and prospects

This paper assessed the relevancy of the DEM for RE walls. The process of identifying thirteen parameters of the DEM was presented. The study showed that the DEM with the Mohr-Coulomb model reproduced the failure mode better than the FEM did (with Mazars' damage model) as shown in a previous study.

The results confirmed that, in the case of vertical loading, interfaces did not have an important effect on the behavior of RE walls. In the case of diagonal loading (which can simulate a seismic case), interfaces should be considered in order to produce better results relative to the ultimate load, the failure modes. However, for the experiments performed in this study, the interface's characteristics varying from 85% to 100% of the corresponding layer characteristics gave satisfactory results. Thus, in practice, the model without interfaces can also be used as the results are sufficiently precise

and can be calculated faster. This finding confirms the results presented in Bui et al. 2014 [9], where the tensile strengths in earthen layers and at interfaces were similar.

From the mechanical characteristics determined in this study, the following values can be suggested for studies on RE walls:

- For earthen layers, considered homogeneous and isotropic: the tensile strength and the cohesion can be taken to be equal to about 10% of the compressive strength of the earthen layer ($f_t = c_{layer} = 0.1\ f_c$). This result is similar to that presented in Bui et al. 2014 [9]. The friction angle of about 50° of the earthen layer (φ_{layer}=50°) can be taken. This result is also on the same order of the results of Cheah et al. 2012 [11] and Bui et al. 2014 [9]. The dilatancy angle of the earthen layer can be taken at Ψ_{layer}=12° but this parameter did not play an important role in the case of RE walls under in-plane loading. However, it would be interesting to study the importance of this parameter for out-plane loading (wind, earthquake).
- For interfaces: cohesion, tensile strength, and friction angle of interfaces of about 85-100% of the respective values of earthen layer should be taken. A dilatancy angle of of 12° of the interface can be taken. Interface stiffness of k_n = 60GPa/m (so k_s=24.59GPa/m) can be taken.

The ultimate load and failure mode are well reproduced thanks to the choosen material model, but nonlinear behavior before the peak is difficult to reproduce numerically. Compatibility conditions at material and non-material interfaces are expected to play an important role and may be related with some instabilities which play an important role in local damage initiation at phase interfaces, as discussed for example in [32] and [33].

It is important to note that while the present paper is prepared, another article was rencently published (Miccoli et al., 2014 [22]). The aim of that study is very similar to our investigation (study the parameters of RE walls); but in that paper, the authors used the finite element method with interface elements. Their results were very similar to the findings in our manuscript by DEM, that confirmed the the results presented in our paper.

In the futur studies, other numerical models will be tested in oder to improve the non-linear part of the diagonal tests that was not yet perfectly reproduced in the present study. In particular, the useful ideas presented in [34] and [35] for modelling delamination and friction where taken into account to simulate the relative displacement phenomena at the interfaces between the different layers formed in the ramming

process, where damaged bands can be formed. The detection of eventually formed shear bands or localized damage band in rammed earth can be envisaged by means of the methods and models presented in [36-37].

References

[1] Allinson D, Hall M. "Hygrothermal analysis of a stabilised rammed earth test building in the UK", *Energy and Buildings* 42, p. 845–852, 2010.

[2] ASTM. Standard test method for diagonal tension (shear) in masonry assemblages (ASTM E519). *American society for testing and materials*, West Conshohocken, PA; 2002.

[3] Bui Q B, Morel J C, Reddy B V V, Ghayad W. "Durability of rammed earth walls exposed for 20 years to natural weathering", *Building and Environment,* vol. 44 (5), p. 912-919, 2009.

[4] Bui Q B, Morel J C, Hans S, Meunier N. "Compression behaviour of nonindustrial materials in civil engineering by three scale experiments: the case of rammed earth", *Materials and Structures,* vol. 42, N° 8, p. 1101-1116, 2009.

[5] Bui Q B, Morel J C. "Assessing the anisotropy of rammed earth", *Construction and Building Materials*, 23, pp. 3005-3011, 2009.

[6] Bui Q B, Morel J C, Hans S, Do A-P. "First exploratory study on dynamic characteristics of rammed earth buildings", *Eng. struct.*, p. 3690-3695, 2011

[7] Bui Q B, Morel J C, Hans S, Walker P. "Effect of moisture content on the mechanical characteristics of rammed earth", *Construction and Building Materials,* 2014 *(in press).*

[8] Bui T T, Limam A. "Masonry Walls under Membrane or Bending Loading Cases: Experiments and Discrete Element Analysis". *Proceedings of the Eleventh International Conference on Computational Structures Technology*, Civil-Comp Press, Stirlingshire, UK, Paper 119, 2012.

[9] Bui T T, Bui Q B, Limam A, Maximilien S. "Failure of rammed earth walls: from observations to quantifications". *Construction and Building Materials*, 51, 295–302, 2014.

[10] Bui T T, Limam A, Bui Q B. "Characterization of vibration and damage in masonry structures: experimental and numerical analysis". *European Journal of Environmental and Civil Engineering*, 2014.

[11] Cheah J S J, Walker P, Heath A, Morgan T K K B. "Evaluating shear test methods for stabilised rammed earth", *Construction Materials*, Volume 165, Issue CM6, p. 325–334, 2012.

[12] Ciancio D, Robinson S. "Use of the Strut-and-Tie Model in the Analysis of Reinforced Cement-Stabilized Rammed Earth Lintels", *Journal of Materials in Civil Engineering*, Vol. 23, No. 5, May 1, 2011

[13] Ciancio D, Augarde C. "Capacity of unreinforced rammed earth walls subject to lateral wind force: elastic analysis versus ultimate strength analysis", *Materials and Structures*, Vol. 46, 2013, Pages 1569–1585

[14] Clough RW, Penzien J. "Dynamics of structures". *Berkeley: Computers &Structures Inc;* 1995, 746p.

[15] Cundall P. A., "A computer model for simulating progressive, large scale movements in blocky rock systems", Proc. Int. Symp. Rock Fracture, ISRM, Nancy, Vol. 1, Paper II–8, 1971a.

[16] Cundall P. A., "The measurement and analysis of acceleration in rock slopes", Ph.D. Thesis, Imperial College of Science and Technology, University of London, 1971b.

[17] Fodde E. “Traditional earthen building techniques in Central Asia”, *Int. J. of Architectural Heritage*, 3, pp. 145-168, 2009.

[18] Gomes M I, Lopes M, Brito J. “Seismic resistance of earth construction in Portugal”, *Engineering Structures*, Volume 33, Issue 3, Pages 932-941, 2011.

[19] Itasca, 3DEC – Three Dimensional Distinct Element Code, Version 4.1, Itasca, Minneapolis, 2011.

[20] Lourenço P B, Oliveira D V, Roca P, Orduna A. “Dry Joint Stone Masonry Walls Subjected to In-Plane”, *Journal of Structural Engineering*, Vol. 131, No. 11, 1665-1673, 2005.

[21] Maniatidis V, Walker P. "Structural Capacity of Rammed Earth in Compression", *Journal of Materials in Civil Engineering*, Vol. 20, No. 3, p. 230-238, 2008.

[22] Miccoli L, Oliveira D V, Silva R A, Muller U, Schueremans L. “Static behaviour of rammed earth: experimental testing and finite element modeling”, *Materials and Structures*, online 3 Sept. 2014.

[23] Morel J C, Mesbah A, Oggero M and Walker P. "Building houses with local materials: means to drastically reduce the environmental impact of construction", *Building and Environment*, 36, pp. 1119-1126, 2001.

[24] Lemos, J.V., “Discrete element modelling of masonry structures”, *International Journal of Architectural Heritage*, Vol. 1(2), 2007, pp. 190-213.

[25] Reddy B.V. V., Kumar P. P. “Embodied energy in cement stabilised rammed earth walls”, *Energy and Buildings*, Volume 42, Issue 3, Pages 380–385, 2010.

[26] Silva R.A., Oliveira D.V., Miranda T., Cristelo N., Escobar M.C., Soares E. “Rammed earth construction with granitic residual soils: The case study of northern Portugal”, *Construction and Building Materials*, Vol. 47, October 2013, Pages 181-191.

[27] Standards NZ. “NZS4297:1998, Engineering design of earth buildings”. *Standards NZ*, Auckland, New Zealand, 1998.

[28] Shyshko S., Mechtcherine V., “Developing a Discrete Element Model for simulating fresh concrete: Experimental investigation and modelling of interactions between discrete aggregate particles with fine mortar between them”, *Construction and Building Materials*, Volume 47, October 2013, Pages 601-615.

[29] Tran V.-H., Vincens E., Morel J.-C., Dedecker F., Le H.-H. “2D-DEM modelling of the formwork removal of a rubble stone masonry bridge”, submitted in *Engineering Structures.*

[30] Vermeer, P. A., de Borst, R.: “Non-associated plasticity for soils, concrete and rock”. Heron 29 (1984) 1–64

[31] Walker P, Keable R, Martin J, Maniatidis V. "Rammed earth-Design and construction guidelines", *BRE Bookshop*, 2005.

[32] Eremeyev, V. A., & Pietraszkiewicz, W. (2011). “Thermomechanics of shells undergoing phase transition”. Journal of the Mechanics and Physics of Solids, 59(7), 1395-1412.

[33] Pietraszkiewicz, W., Eremeyev, V., & Konopińska, V. (2007). Extended nonlinear relations of elastic shells undergoing phase transitions. ZAMM-Journal of Applied Mathematics and Mechanics/Zeitschrift für Angewandte Mathematik und Mechanik, 87(2), 150-159.

[34] Massimo, C., Contrafatto, L., and Greco, L. "A variational model based on isogeometric interpolation for the analysis of cracked bodies." International Journal of Engineering Science 80 (2014): 173-188.

[35] Cazzani, A., Malagù M., and Turco, E. "Isogeometric analysis: a powerful numerical tool for the elastic analysis of historical masonry arches." Continuum Mechanics and Thermodynamics (2014): 1-18. 10.1007/s00161-014-0409-y

[36] Madeo, A., Luca P. and Giuseppe R. "Towards the Design of Metamaterials with Enhanced Damage Sensitivity: Second Gradient Porous Materials." Research in Nondestructive Evaluation 25.2 (2014): 99-124.

[37] Dell'Isola, F., and Kolumban H. "A qualitative analysis of the dynamics of a sheared and pressurized layer of saturated soil." Proceedings of the Royal Society of London. Series A: Mathematical, Physical and Engineering Sciences 454.1980 (1998): 3105-3120.